GEOMATICS AND ENVIRONMENTAL ENGINEERING • Volume 16 • Number 3 • 2022

https://doi.org/10.7494/geom.2022.16.3.5

Pietro Belba[1], Spartak Kucaj[2], Jorgaq Thanas[3]

Monitoring of Water Bodies and Non-vegetated Areas in Selenica – Albania with Sar and Optical Images

Abstract: The availability of Sentinel satellites for providing open data with optical and SAR imagery leads to better opportunities related to Earth surface mapping and monitoring. Recently, optical fusion with radar data has shown improvement in classification quality and the accuracy of information acquired. In this setting, the main objective of this research is to monitor the environmental impact of an open-pit mine on water, vegetation, and non-vegetation areas by exploring the single and combined use of Sentinel-1 and Sentinel-2 data. The data utilized in this paper were collected from the European Space Agency Copernicus program. After selecting the Selenica region, we explored the products in the Sentinel Application Platform. According to our data, Sentinel-2 misses the small water ponds but successfully identifies the river and open-pit areas. It mistakenly identifies urban structures and cloud areas as non-vegetated and does not identify non-vegetated areas which correspond to mining operation areas. Sentinel-1 identifies very small water ponds and delivers additional information in the cloudy areas, but misses a part of the river. Alongside the strong contribution in identifying the vegetation, it also roughly identifies the non-vegetation areas of mining operations.

Keywords: SAR image, optical image, collocated image, water bodies, NDVI, Sentinel images

Received: 22 December 2021; accepted: 25 March 2022

[1] Polytechnic University of Tirana, Faculty of Geology and Mining, Department of Mineral Resources Engineering, Tirana, Albania, email: pietro.belba@fgjm.edu.al

[2] Polytechnic University of Tirana, Faculty of Geology and Mining, Department of Mineral Resources Engineering, Tirana, Albania, email: spartak.kucaj@fgjm.edu.al

[3] Polytechnic University of Tirana, Faculty of Geology and Mining, Department of Mineral Resources Engineering, Tirana, Albania, email: jorgaq.thanas@fgjm.edu.al

1. Introduction

The term "remote sensing" means sensing the surface of the Earth from space by utilizing the features of electromagnetic waves emitted, reflected, or diffracted by the sensed objects with the purpose of the exploration and protection of the environment. There are two types of remote sensing technology: active and passive remote sensing. Passive sensors use the sun's energy and detect the reflected energy from the surface of the Earth. In contrast, active sensors first emit energy and then detect and measure the electromagnetic radiation backscattered from the objects [1, 2].

The state of the art in the research has progressed impressively in the last decade. According to our literature review, one of the alternatives described for enhancing the accuracy of final results is the inclusion of optical indexes of vegetation, soil, and water to increase the training data range and improve overall efficacy [3–6]. Multispectral Sentinel-2 data are mainly used through the application of a threshold on spectral indices that have been proposed worldwide: the Normalized Difference Vegetation Index (NDVI), the Normalized Difference Water Index (NDWI), and the Modified NDWI (MNDWI) to classify water pixels, among others [7–9]. On the other hand, the NDWI index can be used mainly for clear water spectra, and is thus limited in terms of contaminated water bodies (a variety of spectra) like the mining environment [10].

Over the last decade, several studies have highlighted the potential key role of satellite data in ecology, particularly the Normalized Difference Vegetation Index (NDVI) since potentially it is a cheap, systematic, repeatable, and verifiable monitoring method for environmental management [11]. Specifically, it has recently been proposed that monitoring remotely assessed ecosystem functional attributes through NDVI provides an excellent opportunity to assess the effectiveness of management practices and the effects of global environmental changes [12]. Some studies focus on the types of mine vegetation and the relationship between the growth of the mine vegetation and the surrounding soil and heavy metals. They have also monitored the situation of mine environmental restoration [13–15].

The availability of the Sentinel satellites for providing open data with optical and SAR imagery leads to better opportunities related to Earth surface mapping and monitoring. A general definition of image fusion is given as: "Image fusion is the combination of two or more different images to form a new image by using a certain algorithm" [2]. Although radar polarization may be a barrier in identifying some features, this product does not have the presence of atmospheric obstacles, such as clouds [16–18]. Recently, data fusion processes of optical with radar products have been applied to improve classification quality and accuracy. The proposed mapping approach has the main advantages of combining the all-weather capability of the radar sensor with the spectrally rich information from the visible-near infrared spectrum. The synergetic use between optical and radar data is not only

a recognized alternative for urban areas studies [19–21]. Analyzing spatio-temporal characteristics of land-use change are essential for understanding and assessing the ecological consequence of mining [22]. Moreover, the effect of image fusion has an impact on vegetation index quality [23, 24]. Results from many researchers show that Sentinel-1 cross-polarized VH backscattering coefficients have a strong vegetation contribution and are well correlated with the Normalized Difference Vegetation Index (NDVI) values retrieved from optical sensors [25–28].

In this setting, the main objective of this study was to evaluate the environmental impact of the open-pit mine in water and non-vegetation area by exploring the information gained by the combination of Sentinel-1 and Sentinel-2 data. The specific objectives consist of applying histogram analysis for the Sentinel-2 part and scatterplot analysis for Sentinel-1 part in the collocated image.

The main hypothesis is that we achieve more detailed terrain information by means of the combination of Sentinel-1 and Sentinel-2 data.

2. Materials

2.1. Study Area

The Selenica bitumen mine is located in Selenica county and Vlora district in Albania (Fig. 1).

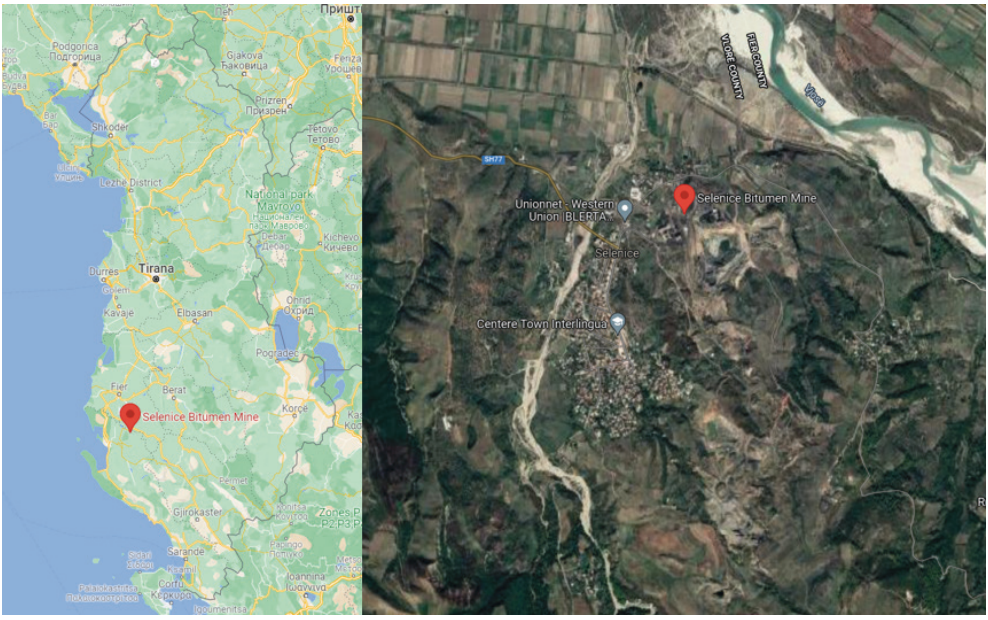

Fig. 1. Location of the Selenica open pit mine in Albania
Source: Google Maps

The history of the Selenica deposit of natural bitumen in Albania spans over 2000 years. The natural bitumen originating from the deposit, named Selenizza®SLN, belongs to the group of natural asphaltites which include Gilsonite, Trinidad, etc. It is an additive for modifying road paving bitumen and creating high-performance asphalt mixes. The Selenica mine is a rare deposit that contains a large amount of natural bitumen. Ore extraction is performed via open-pit mining using excavators, and the product is practically unalterable in the environment. It is not considered dangerous for terrestrial plants and aquatic organisms [29].

2.2. Data Set

The data utilized in this paper were collected from the European Space Agency (ESA) Copernicus program, which comprises five satellite families, each one focusing on a specific aspect of the observation of the earth. For this study, we have used data from Sentinel-2 and Sentinel-1 missions, and for accessing Sentinel data, we have used the Copernicus Open Access Hub [30, 31].

Sentinel-1 is a radar satellite launched by the ESA operating at C-Band Synthetic Aperture Radar (SAR) instrument operating at a center frequency of 5.405 GHz comprises a constellation of two polar-orbiting satellites, operating day and night performing C-Band synthetic aperture radar imaging. A radar image results from the reconstruction of the echoes recovered in the antenna after the emission of microwave pulses which is called backscattering. The radar image formation from the recorded echoes is done in the sensor reference system composed of the azimuth and range axis. The azimuth axis is the direction along which the satellite travels, while the range axis is the direction across the satellite travels, the beam projection. It measures the intensity of the returned signal, which was actively sent to the Earth's surface. It supports operations in single (HH or VV) or dual polarization with four acquisition modes, and the products are SAR level-0, Level-1 SLC, Level-1 GRD, and Level-2 OCN. This allows the mapping of physical characteristics, such as roughness, moisture, and structure of the surfaces. Furthermore, radar images can also be acquired through cloud cover and independent of daylight.

Sentinel-2 is a multispectral satellite operating in the visible and infra-red spectrum (nanometer scale). The Copernicus Sentinel-2 mission comprises a constellation of two polar-orbiting satellites placed in the same sun-synchronous orbit, phased at 180° to each other. It is a passive sensor that measures the energy emitted from the Earth's surface in 13 separate bands at three different spatial resolutions (10, 20, and 60 m). The spatial resolution depends on the particular spectral band and requires daylight and cloud-free conditions.

2.3. Extraction of Data

In this paper, we have searched in the Copernicus Access Open Hub for the sensing period 1.06.2020 to 30.06.2020, for Sentinel-1 product type GRD, sensor mode IW while for Sentinel-2 product type S2MSI2A, cloud cover [0 TO 2], and we

have found two images which cover Selenica region (Fig. 2). There was a difference of eight days since the acquisition period for the Sentinel-1 and the Sentinel-2 images. However, it was hypothesized that both indices were obtained at the same water and vegetation phenological status.

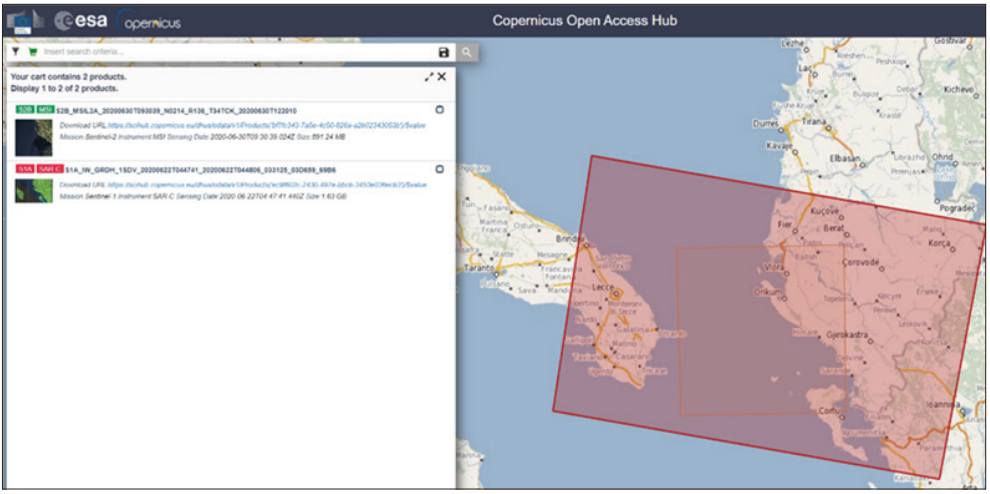

Fig. 2. Search in the Copernicus Open Access Hub for image products from Sentinel-1 and Sentinel-2 satellites covering Selenica region

3. Methods

Our method consists of combining the two scenes for using complementary information using the collocation algorithm in the Sentinel Application Platform.

3.1. Preprocessing

After selecting the region of interest for our study (the Selenica region), we explored the Sentinel-1 and Sentinel-2 products in the Sentinel Application Platform (SNAP), which is a common architecture for all Sentinel Toolboxes [32]. The workflow for Sentinel-2 image consists of preprocessing only by creating a subset. The workflow for Sentinel-1 image was a more detailed preprocessing beginning with the creating a subset than performing radiometric calibration and speckle filtering, conversion to decibel scale, and the terrain correction and calculation of a band ratio, which is optional [33].

3.2. Collocation

In a second stage, we collated the two images where there would be the fusion process of SAR data (in the master product) with optical imagery (in the slave product). When products were collocated, a new product was created, which contained a copy

of all components of the master product, i.e., band data, tie-point grids, flag codings, bitmask definitions, and metadata. The band data of the slave products were resampled into the geographical raster of the master product. The collocation algorithm requires accurate geopositioning information for both master and slave products. As for the master product, the tie-point grids, flag codings, and bitmask definitions of the slave products were copied. Slave product metadata were not transferred [32].

3.3. Analyzing the Histogram for NDVI in Sentinel-2 Part of the Collocated Image

To identify water bodies and non-vegetated areas in the Sentinel-2 part, we applied the NDVI, observed the histogram, and extracted our mask for the water bodies and the non-vegetated areas; we created these masks by using as threshold the NDVI value, using the Mask Manager and converting the mask into a layer. The NDVI was computed according to state of the art thresholds. It was computed by Band Maths as (NIR – Red)/(NIR + Red) where NIR and Red were considered the amount of near-infrared and red light, respectively, reflected by a surface and measured by satellite sensors. Normalized Difference Vegetation Index (NDVI) was used for vegetation cover analysis. This index measures primary productivity quantitatively, allowing an estimation of vegetation health [34]. Bare soil, cloud, snow, and concrete have NDVI values close to zero, while water has negative NDVI values [35].

3.4. Analyzing the Scatter Plot of the Polarization Bands in Sentinel-1 Part of the Collocated Image

To identify water bodies and non-vegetation areas in the Sentinel-1 part, we focused on analyzing polarization bands and their ratio. We used the scatter plot selecting the VH band for the x-axis and the VV band for the y-axis to identify water bodies. We used the fact that water surfaces reflect the microwave radiation away from the sensor, so the signal is low in that case. The scatter plot can also be used to extract thresholds for the ratio and the VH band to create a mask for the non-vegetation areas from the Sentinel-1 band, considering that bare soil has a high VV-VH ratio and small VH and VV values.

3.5. Analyzing the Merged Image

To demonstrate the effects of combining Sentinel-1 and Sentinel-2, we compared the above analysis in identifying water bodies and non-vegetation areas.

4. Results

Initially, we will provide the technical aspects of the combination of two images and then monitoring of water bodies as well as non-vegetation areas in the merged product.

4.1. Technical Aspects for Merging Images

First we had to do the preprocessing, which only consisted in creating a subset for the Sentinel-2 image. Utilizing it, we only extracted one very small spatial part of the interest of the whole Sentinel-2 scene, which considerably reduced the file size and limited computation times. This can be done by the command "Raster-Subset". We extracted our subset from the geographic coordinates in the spatial subset tab. In contrast, in the Band subset tab, we only selected Band 1 to Band 12, excluding Band 8A as it is the narrow near-infrared band that is completely within Band 8. At that moment, it was necessary to know the coordinate reference system of the dataset. We would need it later for the projection of the Sentinel-1 scene (in our case here, it was the WGS 84/UTM zone 34N) (Fig. 3).

Fig. 3. Preprocessing for Sentinel-2 image: creating a subset

For the preprocessing of the Sentinel-1 image, a number of steps needed to be followed. To create the subset Sentinel-1 image, we used "Raster-Subset". Similarly, as for the Sentinel-2 scene, we wanted to select our subset from the geographic coordinates (we entered the same coordinates in the Sentinel-2 subset). In that subset, we noticed the mirror effect with the image that we downloaded from Copernicus Open Access Hub. This would serve as an input product for the next preprocessing step.

Radiometric calibration is necessary as recording conditions may vary between dates, so the radiometric calibration corrects these differences and provides comparable pixel values. We used radar-radiometric-calibrate. Radiometric calibration converts backscatter intensity as received by the sensor to the normalized radar cross-section (Sigma0) as a calibrated measure taking into account the global incidence angle of the image and other sensor-specific characteristics. The resulting product will appear to the left in our product explorer as _Cal product, and it will serve as input for the next step.

Speckles are the image's salt and pepper grains that harden their interpretation. They result from random or noisy interference of all the single scatterers within one resolution cell. The speckle filtering by applying filters tries to reduce this noise by

spatial or temporal filtering. Extensive reviews and comparisons of speckle filters are provided by many authors [36–37]. We used the Lee Sigma filter published by Lee et al. [38] which uses two different window sizes to estimate the presence and intensity of speckle. It minimizes the speckle while maintaining sharp edges where they can be detected. To perform speckle filtering, we selected our subset calibrated product, and we used for "Radar-Speckle Filtering-Single Product Speckle Filter". The resulting product will appear to the left in our product explorer as _Spk product, and it will serve as input for the next step.

Conversion to decibel scale is ultimately not required, and it does not change the information content of the image, but it is advisable when image contrasts matter. If we select only one band and look at the statistics, we see that we have a very large range of possible pixel values; however, most of the pixels have very small ones. To stretch the distribution of values more evenly, which in turn then increases our contrast, we can convert that band into a logarithmic scale. We now have two virtual bands that are not written on the hard disk. However, these bands can be used as inputs for the next preprocessing step.

The last step is the terrain correction which applies a Digital Elevation Model (DEM) to the Sentinel-1 scene and corrects the geometric distance distortions which result from the topography and the recording geometry of the Sentinel-1 sensor. To perform the correction, we go for "Radar-Geometric-Terrain Correction-Range Doppler Terrain Correction". We chose our newly created decibel bands in the processing parameters, and for the map projection, we used a predefined coordinate reference system. We selected the one we noted from the Sentinel-2 product (WGS 84/UTM zone 34N). Terrain correction will geocode the image by correcting SAR geometric distortions using the DEM and producing a map projected product. Only now do we not see the mirror effect of the image. Our resulting product will appear in the product explorer as _TC.

The optional calculation of a band ratio is the next step. To reduce the imbalance of the Bands (2 for Sentinel-1, 13 for Sentinel-2), a ratio is calculated between the two polarizations using the Band Math's operator. Figure 4 presented the preprocessing for the Sentinel-1 image.

We used the command "Raster-Geometric-Collocation" to merge the preprocessed Sentinel-2 and Sentinel-1 scenes. In the master product, we chose our Sentinel-1 product as it has highly precise geocoding due to the application of our digital elevation model. In contrast, for the slave product whose pixels were reprojected onto the coordinate system of the master product, we chose the Sentinel-2 product with the bilinear interpolates resampling method. If we check the bands of our product, we have the 12 bands from the Sentinel-2 product and our decibel bands from Sentinel-1 product. For a first overview, we chose band 4 and 3 from Sentinel-2, and for the blue channel, the VV band from Sentinel-1 product. Depending on the different sensors' recording directions and geometry, these do not completely overlap (Fig. 5).

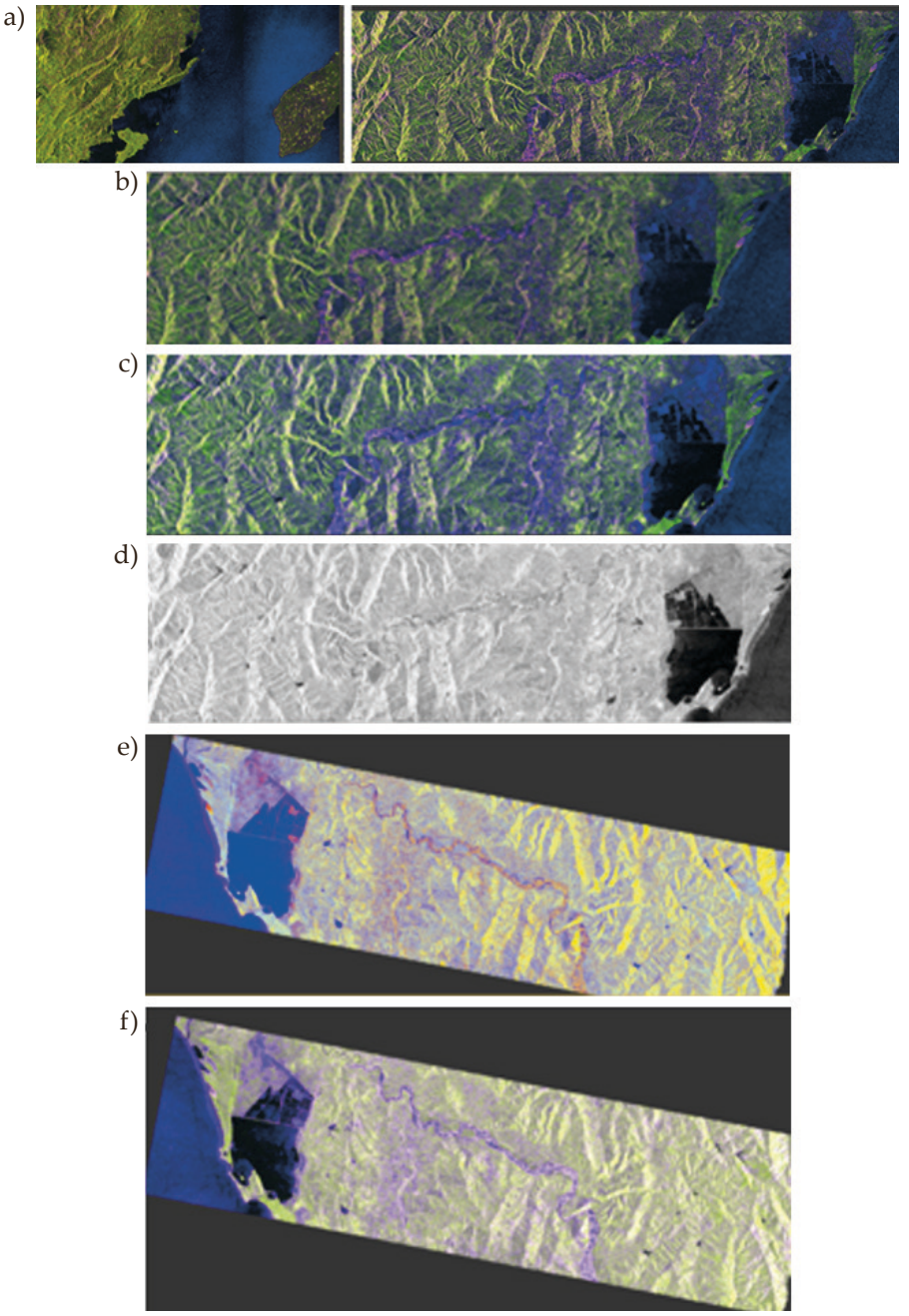

Fig. 4. Preprocessing for Sentinel-1 image: a) creating a subset (the whole image in the left and after the subset in the right); b) the radiometric calibration; c) the speckle filtering; d) conversion to decibele scale; e) the terrain correction; f) the calculation of a band ratio (optional). The mirror effect disappears after the terrain correction

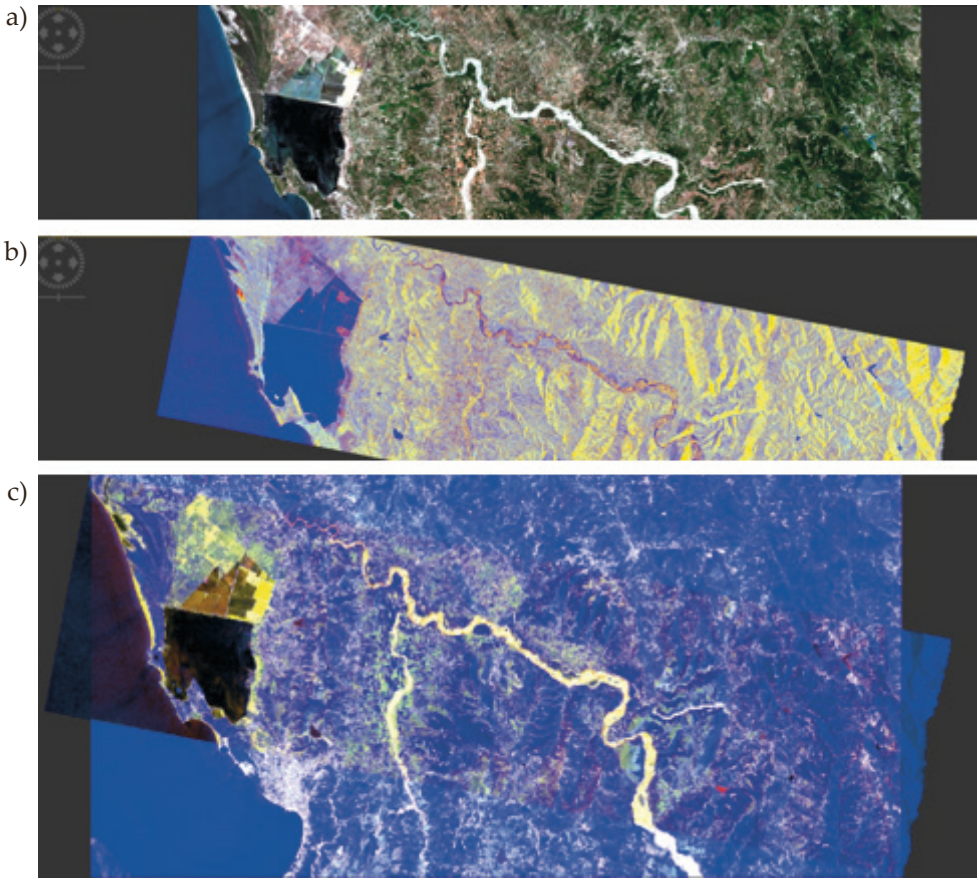

Fig. 5. The preprocessed Sentinel-1 image (a), Sentinel-2 image (b) and the merged product (c)

4.2. Monitoring of Water Bodies as Well as Non-vegetated Areas in the Merged Product

We aim to identify the water surfaces of the tailing ponds and the non-vegetated areas of the Selenica region. Initially, by doing these identifications independently for the Sentinel-1 (S1) and Sentinel-2 (S2) bands and then comparing both results in a second step where the added value becomes more apparent. Open SNAP and start with our combined S1 and S2 products as collocated.

Firstly we want to identify water bodies and non-vegetated areas in the Sentinel-2 part of the collocated image. For this, we use the NDVI to identify water bodies and the vegetated and non-vegetated areas at once [39]. This is because, in the RGB view of the subset, we worked with pins for different spectra and observed for the vegetation spectra the high reflectance and the low reflectance (Fig. 6).

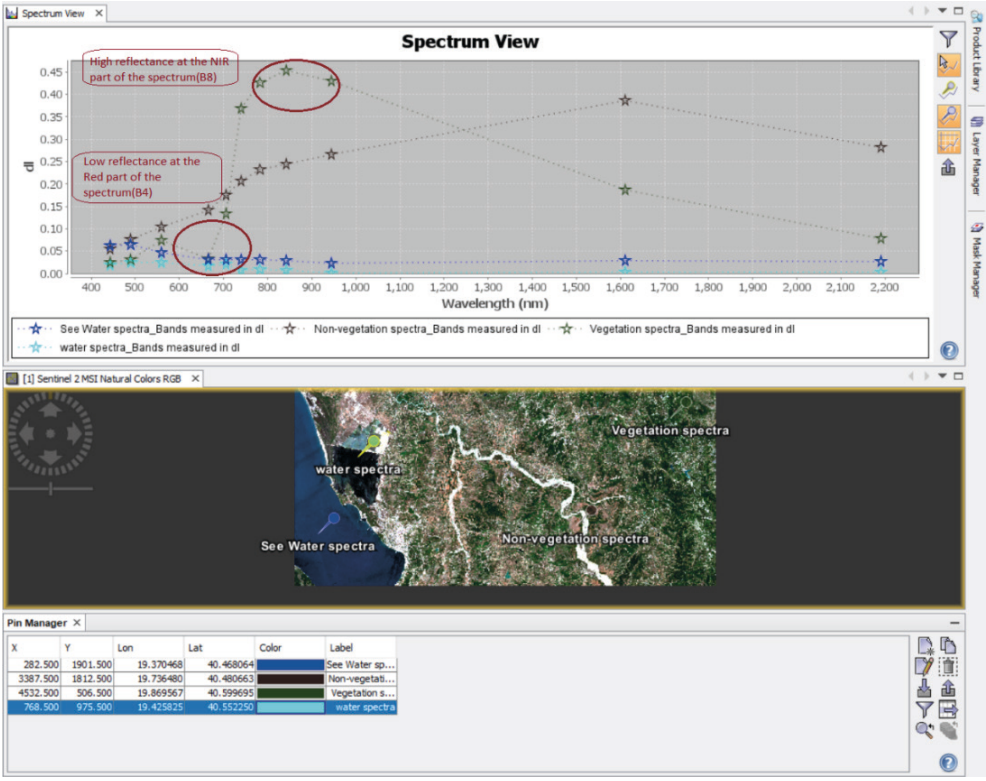

Fig. 6. Exploring the spectral information of the region of interest

In Band Maths we created the NDVI Band: "Raster – Band Maths, Name: NDVI". The expression is the difference between B8 and B4 (we normalize by dividing by their sum). As a result, a greyscale image will be created. We want to extract the water bodies and non-vegetated areas by thresholding these NDVI values. We can illustrate that by choosing masks from the histogram. NDVI has negative values for water bodies, intermediate values (0.0–0.5) for non-vegetated or bare soil areas, and large values towards 1 for vegetated areas. By thresholding the NDVI values using the Mask Manager, we converted the mask into a layer. Firstly we have created the mask for the water bodies named S2_water (NDVI should be smaller than −0.05), then, in the same way, we continue with creating the mask for the non-vegetated areas or bare soil areas named S2_non_veg (NDVI > −0.05 and NDVI < 0.5).

In our image, we can see the water mask in blue for the river and also the water bodies as well as water in the areas where mining operations are no longer present. As a result, we can identify the water ponds as well as the river. But there is no view in the regions with clouds and no view of the very small water ponds.

From the mask for the non-vegetated area, we see the mine masked to identify the open pit areas, but we have some urban structures masked as non-vegetated

areas. Compared with our natural color view (RGB), even the clouds are identified as non-vegetated areas. We have no identification of exactly the non-vegetated areas corresponding to mining operation areas. Figure 7 presented the application of the water mask and the non-vegetated mask in the Sentinel-2 part of the collocated image.

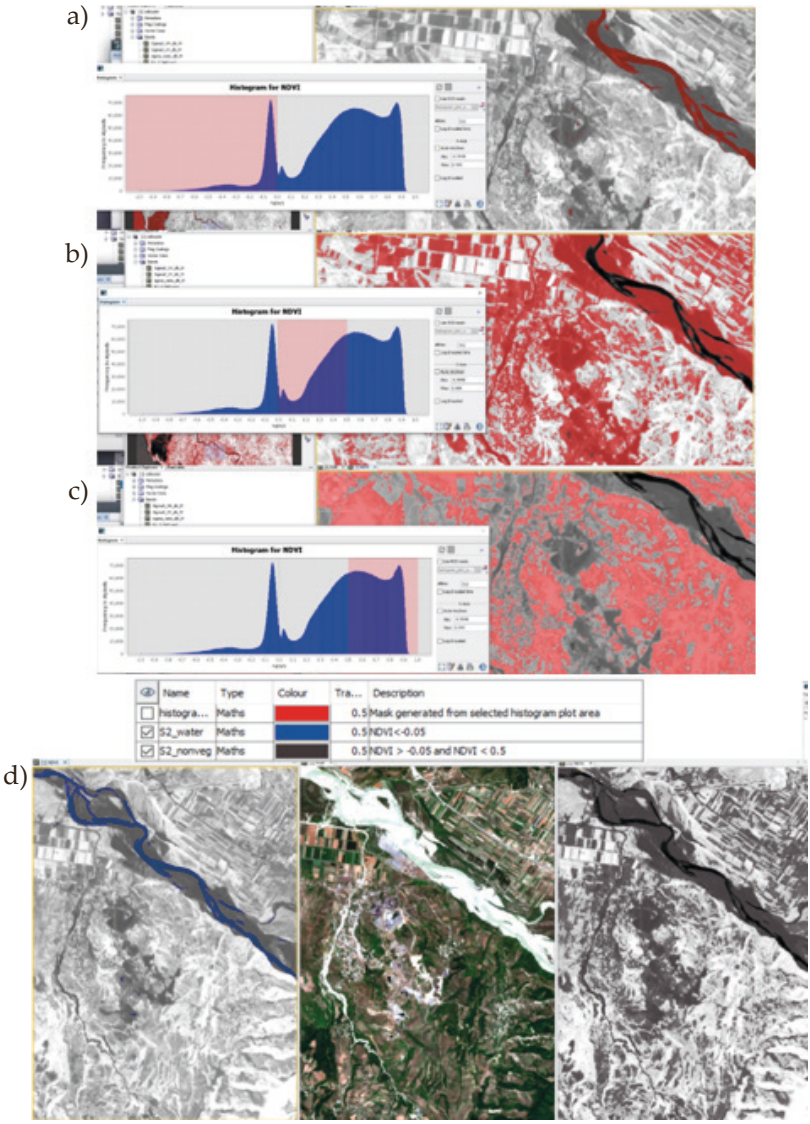

Fig. 7. Choosing masks from the histogram (a, b, c) and application in the Sentinel-2 part of the collocated image (d): the mask for water bodies (NDVI < −0.05) in the left; the mask for the non-vegetated areas or bare soil areas (NDVI > −0.05 and NDVI < 0.5) in the right; natural color view (RGB) in the middle

Secondly, we aimed to identify water bodies and non-vegetated areas in the Sentinel-1 part of the collocated image and therefore we continued creating the water mask for the Sentinel-1 bands. We made use of the fact that water surfaces specularly reflect the microwave radiation away from the sensor, so the signal is low in that case. We can illustrate that by choosing the scatterplot selected bands from Sentinel-1 where the VH band stands for the x-axis and the VV band for the y-axis.

In the scatter plot, we can see the VH and VV values distribution. We can see that the majority of the values are centered around −20 dB or lower for the VH polarization and −15 dB or lower for the VV polarization. We set these values in Band Math, then create the mask in Mask Manager, and we can see the water bodies in light blue in our image (Fig. 8).

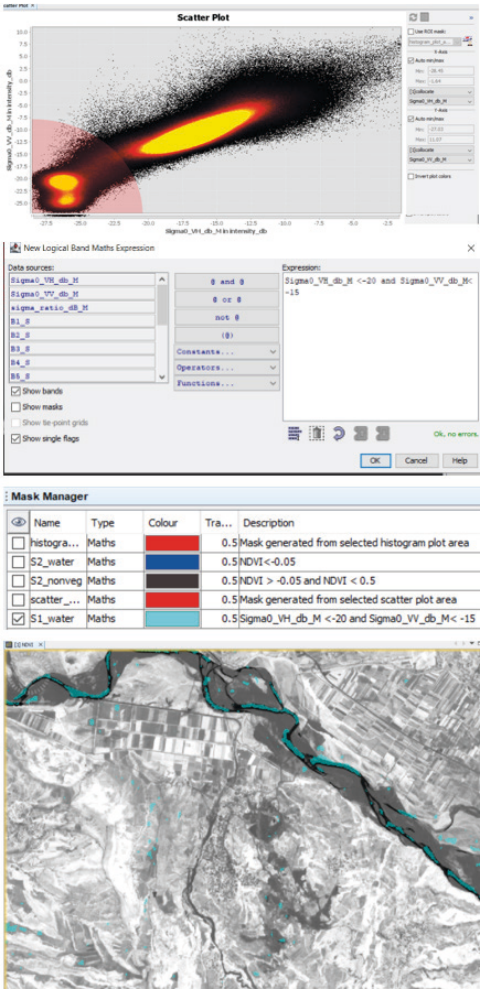

Fig. 8. Application in the Sentinel-1 part of the collocated image the mask for water bodies

In the next step, we aim to create a mask for the non-vegetated areas from the Sentinel-1 bands. We exploit that bare soil has a high VV-VH ratio and small VH and VV values. From the scatter plot, the surface soil cover is characterized by back-scatter values of around −17 dB or lower for the VH polarization and 6 dB or greater for the sigma ratio. We set these values in Band Math then create the mask in Mask Manager and see that the bare soil is dark brown in our image (Fig. 9).

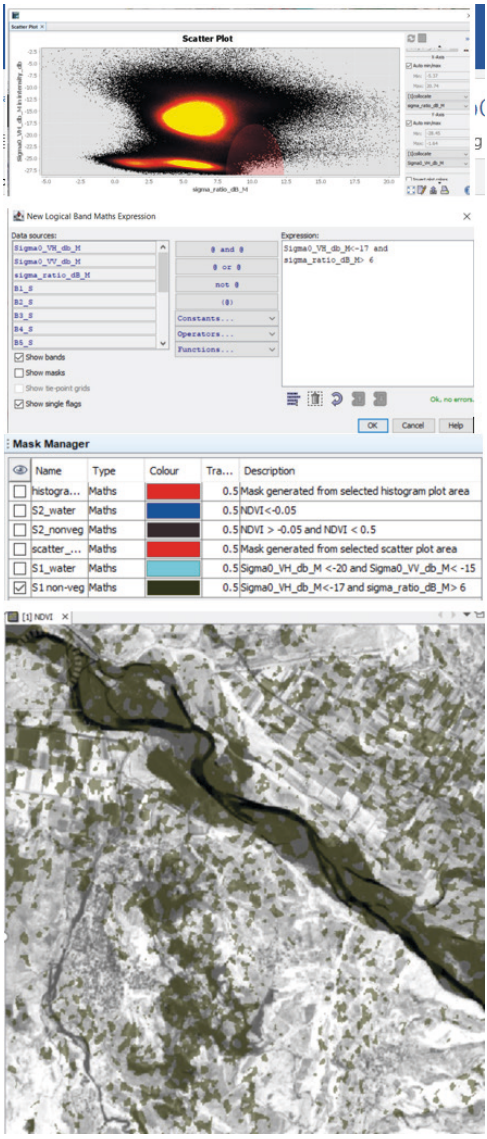

Fig. 9. Application in the Sentinel-1 part of the collocated image the mask for non-vegetated areas

Figure 10 shows the application of a water mask for both Sentinel-1 and Sentinel-2 images. The Sentinel-2 water mask cannot identify small ponds but successfully identified the river, while for a cloudy area, no information was present. After we added a water mask from Sentinel-1, it missed a part of the river, but it identified the water ponds in the cloudy area, and it also identified the very small water ponds.

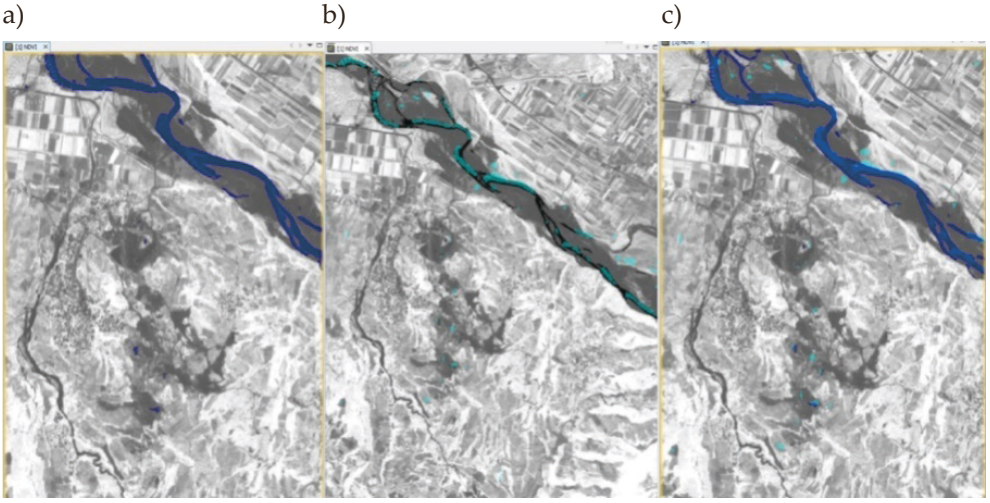

Fig. 10. Application of the mask for water bodies:
a) Sentinel-2 part (blue color); b) Sentinel-1 part (light blue);
c) both masks (blue color for Sentinel-2 and light blue for Sentinel-1)

Figure 11 reveals the mask application for non-vegetated areas for both Sentinel-1 and Sentinel-2 images.

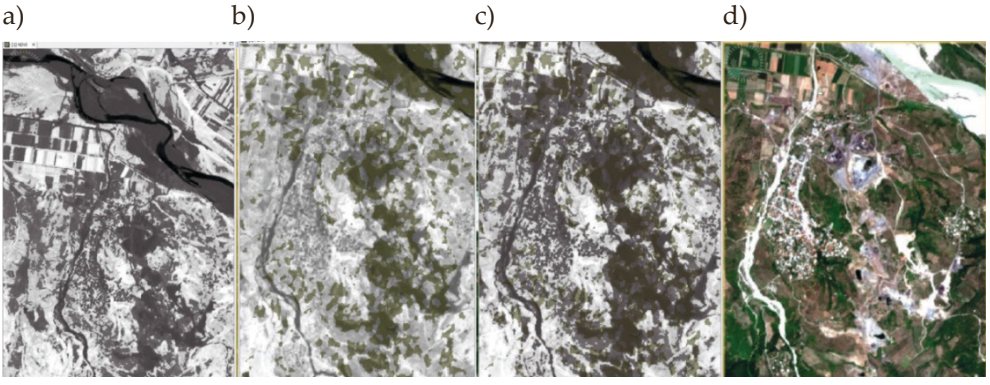

Fig. 11. Application of the mask for non-vegetated areas: a) Sentinel-2 part;
b) Sentinel-1 part; c) collocated image with both masks; d) RGB part

We can see that the mask in the Sentinel-2 part successfully identifies the open pit areas that are not vegetated and identifies urban structures as non-vegetated (further refinement would be needed to identify only areas that correspond with mine operations), wrongly identifying the cloudy area as non-vegetated area. Adding in the Sentinel-1 non-vegetated mask can help to roughly identify the non-vegetated areas of mining operations and correct the view of the non-vegetated areas in the cloudy part.

5. Discussion

Remote sensing has become a routine approach for land surface water bodies and vegetation monitoring because the acquired data can provide high-quality information, which is substantially different from conventional in situ measurements [40, 41]. Various methods, including unsupervised and supervised classification and spectral water indexes, have been developed to extract water bodies from different remote sensing images. The combination of Sentinel-1 and Sentinel-2 scenes helps monitor the water bodies and non-vegetated areas because we can obtain microwave information (Sentinel-1 different polarization bands) and visible/infrared information (Sentinel-2 – 12 bands) having a broad wave data and using their complementary information content.

We used the NDVI in this study not to study vegetation but to exclude it as our study aimed to identify water bodies and non-vegetation areas. The NDVI values varied between −1 to +1. With the increase of vegetation cover, the value increased to +1. At the same time, non-vegetated areas were close to 0 and negative for the NDVI in water bodies.

For the identification of water bodies, we don't use the NDWI index because this can mainly be used for clear water spectra and is limited by contaminated water bodies (variety of spectra) like the mining environment [10]. In this study, we have used NDVI in Sentinel-2 scene because it helps us identify the water and soil (non-vegetated areas) simultaneously. In our study, just like other authors, the use of NDVI helped us at the same time in the identification of water bodies as well as the non-vegetation areas concretely open pit areas in the optical part of the collocated image [25]. The Sentinel-2 image study, according to the authors but also our own data, can identify cloudy areas like non-vegetated ones [27].

In the Sentinel-1 scene, we observed that water and flat bare soil have low VH and VV but a large VH/VV ratio, which helped us set the correct values while converting the masks into layers in Mask Manager. This finding is following the literature [42–44]. Co-polarized (e.g., the same transmitted and received polarizations) polarization radar data (HH, VV) are more suitable for water cover detection [45, 46].

According to some authors, the backscatter of floodwater in HV and VH is the same, and both HV and VH polarizations are adequate for mapping floodwater [42]. From our scatterplot and literature, the surface water cover is characterized by backscatter values of around −20 dB or lower for the VH polarization and −15 dB or lower for the VV polarization [42, 43].

The possibility of using a high temporal and spatial resolution of the Sentinel-1 (S1) imagery motivated the authors to develop the methodology for its retrieval based on backscattering coefficient (σ°), as calculated from the VH and VV polarizations [44]. Our scatterplot and literature show that the surface soil cover is characterized by backscatter values of around −17 dB or lower for the VH polarization and 6 dB or greater for the sigma ratio [44].

6. Conclusions

Both water masks from the Sentinel-1 and Sentinel-2 images have their advantages and disadvantages; however, the great potential of the merged product is that we can use that information to better understand the bigger picture. The merged product can serve as a new image with numerous characteristics from Sentinel-1 and Sentinel-2 images.

According to our data, Sentinel-2 misses the smallest water ponds; however, it successfully identifies the bigger water ponds and the river. It has no information for cloudy areas. Meanwhile, Sentinel-1 misses a part of the river, but it identifies the smallest water ponds and gives additional information regarding the water ponds of the cloudy areas.

The non-vegetated mask from Sentinel-2 successfully identifies the open pit areas, the urban structure and also the cloud area as non-vegetated. The non-vegetated mask from Sentinel-1 image has a stronger contribution in identifying the vegetated areas and corrects the non-vegetated ones within the cloudy area. The overall findings indicated that Sentinel-1 and 2 indices could only provide a similar pattern over vegetated areas. The application of the mask for non-vegetated areas tells us that they are complementary to each other. If combined, both optical and radar technologies would help overcome the identified weaknesses of each method by using the benefits of both.

We have identified water and the non-vegetation areas in general. Still, it would be more useful in the future to try to identify the part of non-vegetation which corresponds to mining operations utilizing further refinements. According to our research purpose, the proposed methodology will help in future studies by analyzing the impact of mining on soil properties through the assessment of vegetation status using time-series evaluations.

References

[1] Tempfli K., Kerle N., Huurneman G.C., Janssen L.L.F. (eds.): *Principles of Remote Sensing: An Introductory Textbook*. International Institute for Geo-Information Science and Earth Observation (ITC), Enschede, The Netherlands 2009. http://www.itc.nl/library/papers_2009/general/PrinciplesRemoteSensing.pdf [access: 14.12.2021].

[2] Pohl C., Van Genderen J.L.: *Review article Multisensor image fusion in remote sensing: Concepts, methods and applications*. International Journal of Remote Sensing, vol. 19(5), 1998, pp. 823–854. https://doi.org/10.1080/014311698215748.

[3] Ghosh S.M., Behera M.D.: *Aboveground biomass estimation using multi-sensor data synergy and machine learning algorithms in a dense tropical forest*. Applied Geography, vol. 96, 2018, pp. 29–40. https://doi.org/10.1016/j.apgeog.2018.05.011.

[4] Deus D.: *Integration of ALOS PALSAR and Landsat Data for Land Cover and Forest Mapping in Northern Tanzania*. Land, vol. 5(4), 2016, 43. https://doi.org/10.3390/land5040043.

[5] Akar Ö., Güngör O.: *Integrating multiple texture methods and NDVI to the Random Forest classification algorithm to detect tea and hazelnut plantation areas in northeast Turkey*. International Journal of Remote Sensing, vol. 36(2), 2015, pp. 442–464. https://doi.org/10.1080/01431161.2014.995276.

[6] Sarker M.L.R., Nichol J., Iz H.B., Ahmad B.B., Rahman A.A.: *Forest Biomass Estimation Using Texture Measurements of High-Resolution Dual-Polarization C-Band SAR Data*. IEEE Transactions on Geoscience and Remote Sensing, vol. 51, no. 6, 2013, pp. 3371–3384. https://doi.org/10.1109/TGRS.2012.2219872.

[7] Ma M., Wang X., Veroustraete F., Dong L.: *Change in area of Ebinur Lake during the 1998–2005 period*. International Journal of Remote Sensing, vol. 28(4), 2007, pp. 5523–5533. https://doi.org/10.1080/01431160601009698.

[8] Jain S.K., Singh R.D., Jain M.K., Lohani A.K.: *Delineation of flood-prone areas using remote sensing techniques*. Water Resources Management, vol. 19(4), 2005, pp. 333–347. https://doi.org/10.1007/s11269-005-3281-5.

[9] Xu H.Q.: *Modification of Normalised Difference Water Index (NDWI) to enhance open water features in remotely sensed imagery*. International Journal of Remote Sensing, vol. 27(14), 2006, pp. 3025–3033. https://doi.org/10.1080/01431160600589179.

[10] Dold B.: *Evolution of acid mine drainage formation in sulphidic mine tailings*. Minerals, vol. 4(3), 2014, pp. 621–641. https://doi.org/10.3390/min4030621.

[11] Pettorelli N., Vik J.O., Mysterud A., Gaillard J.-M., Tucker C.J., Stenseth N.C.: *Using the satellite-derived Normalized Difference Vegetation Index (NDVI) to assess ecological effects of environmental change*. Trends in Ecology & Evolution, vol. 20(9), 2005, pp. 503–510. https://doi.org/10.1016/j.tree.2005.05.011.

[12] Alcaraz-Segura D., Liras E., Tabik S., Paruelo J., Cabello J.: *Evaluating the consistency of the 1982–1999 NDVI trends in the Iberian Peninsula across four time-series derived from the AVHRR sensor: LTDR, GIMMS, FASIR, and PALII*. Sensors, vol. 10(2), 2010, pp. 1291–1314. https://doi.org/10.3390/s100201291.

[13] Bao N., Wu L., Liu S., Li N.: *Scale parameter optimization through high-resolution imagery to support mine rehabilitated vegetation classification*. Ecological Engineering, vol. 97, 2016, pp. 130–137. https://doi.org/10.1016/J.ECOLENG.2016.06.117.

[14] Cai X.H., He B.H., Li X.G., Wang L.: *An Investigation of Plants and Vegetation in Some Mine Slag Disposal Yards*. Journal of Southwest University (Natural Science), vol. 32(7), 2010, pp. 101–106.

[15] Wanat N., Joussein E., Soubrand M., Lenain J.-F.: *Arsenic (As), antimony (Sb), and lead (Pb) availability from Au-mine Technosols: A case study of transfer to natural vegetation cover in temperate climates*. Environmental Geochemistry and Health, vol. 36(4), 2014, pp. 783–795. https://doi.org/10.1007/s10653-014-9596-5.

[16] Erinjery J.J., Singh M., Kent R.: *Mapping and assessment of vegetation types in the tropical rainforests of the Western Ghats using multispectral Sentinel-2 and SAR Sentinel-1 satellite imagery*. Remote Sensing of Environment, vol. 216, 2018, pp. 345–354. https://doi.org/10.1016/J.RSE.2018.07.006.

[17] Whyte A., Ferentinos K.P., Petropoulos G.P.: *A new synergistic approach for monitoring wetlands using Sentinels-1 and 2 data with object-based machine learning algorithms.* Environmental Modelling & Software, vol. 104, 2018, pp. 40–54. https://doi.org/10.1016/j.envsoft.2018.01.023.

[18] Clerici N., Valbuena Calderón C.A., Posada J.M.: *Fusion of sentinel-1a and sentinel-2A data for land cover mapping: A case study in the lower Magdalena region, Colombia*. Journal of Maps, vol. 13(2), 2017, pp. 718–726. https://doi.org/10.1080/17445647.2017.1372316.

[19] Haas J., Ban Y.: *Sentinel-1A SAR and sentinel-2A MSI data fusion for urban ecosystem service mapping*. Remote Sensing Applications: Society and Environment, vol. 8, 2017, pp. 41–53. https://doi.org/10.1016/j.rsase.2017.07.006.

[20] Corbane Ch., Faure J.-F., Baghdadi N., Villeneuve N., Petit M.: *Rapid urban mapping using SAR/optical imagery synergy*. Sensors, vol. 8(11), 2008, pp. 7125–7143. https://doi.org/10.3390/s8117125.

[21] Gamba P., Dell'Acqua F., Dasarathy B.V.: *Urban remote sensing using multiple data sets: Past, present, and future*. Information Fusion, vol. 6(4), 2005, pp. 319–326. https://doi.org/10.1016/j.inffus.2005.02.007.

[22] Madasa A., Orimoloye I.R., Ololade O.O.: *Application of geospatial indices for mapping land cover/use change detection in a mining area*. Journal of African Earth Sciences, vol. 175, 2021, 104108. https://doi.org/10.1016/j.jafrearsci.2021.104108.

[23] Ghasemian Sorboni N., Pahlavani P., Bigdeli B.: *Vegetation mapping of sentinel-1 and sentinel-2 satellite images using convolutional neural network and random forest with the aid of dual polarized and optical vegetation indexes*. The International Archives of the Photogrammetry, Remote Sensing and Spatial Information Sciences, vol. XLII-4/W18, 2019, pp. 435–440. https://doi.org/10.5194/isprs-archives-XLII-4-W18-435-2019.

[24] Ghimire P., Lei D., Juan N.: *Effect of image fusion on vegetation index quality – A comparative study from Gaofen-1, Gaofen-2, Gaofen-4, Landsat-8 OLI and MODIS imagery*. Remote Sensing, vol. 12(10), 2020, 1550. https://doi.org/10.3390/rs12101550.

[25] Kotaridis I., Lazaridou M.: *Delineation of Open-Pit Mining Boundaries on Multispectral Imagery*. [in:] Hammond A., Keleher P. (eds.), *Remote Sensing*, IntechOpen, London 2020. https://doi.org/10.5772/intechopen.94120.

[26] Frantz D., Schug F., Okujeni A., Navacchi C., Wagner W., van der Linden S., Hostert P.: *National-scale mapping of building height using Sentinel-1 and Sentinel-2 time series*. Remote Sensing of Environment, vol. 252, 2021, 112128. https://doi.org/10.1016/j.rse.2020.112128.

[27] European Space Agency (ESA): *S2 MPC Level 2A Data, Quality report*. https://sentinel.esa.int/documents/247904/685211/Sentinel-2-L2A-Data-Quality-Report [access: 14.12.2021].

[28] Stendardi L., Karlsen S.R., Niedrist G., Gerdol R., Zebisch M., Rossi M., Notarnicola C.: *Exploiting time series of Sentinel-1 and Sentinel-2 imagery to detect meadow phenology in mountain regions*. Remote Sensing, vol. 11(5), 2019, 524. https://doi.org/10.3390/rs11050542.

[29] *Selenizza® Natural Additive Asphaltite*. https://www.selenizza.eu/selenizza.php [access: 14.12.2021].

[30] European Space Agency (ESA): *Sentinel-2 User Handbook*. https://Sentinels.copernicus.eu/web/Sentinel/user-guides/document-library/-/asset_publisher/xlslt4309D5h/content/Sentinel-2-user-handbook [access: 14.12.2021].

[31] European Space Agency (ESA): *Copernicus Open Access Hub.* https://scihub.copernicus.eu/ [access: 14.12.2021].

[32] European Space Agency (ESA): *SNAP-Science Toolbox Exploitation Platform.* http://step.esa.int/main/toolboxes/snap/ [access: 14.12.2021].

[33] European Space Agency (ESA): *Level 1 Preprocessing*. https://sentinel.esa.int/ja/web/sentinel/level-1-pre-processing-algorithms [access: 14.12.2021].

[34] Rouse J.W., Haas R.H., Schell J.A., Deering D.W.: *Monitoring vegetation systems in the Great Plains with ERTS*. [in:] *Third Earth Resources Technology Satellite-1 Symp., December 10–15 1974, Greenbelt, MD*, paper A20, NASA, Washington 1974, pp. 301–317.

[35] Neigh C.S.R., Tucker C.J., Townshend J.R.G.: *North American vegetation dynamics observed with multi-resolution satellite data*. Remote Sensing of Environment, vol. 112(4), 2008, pp. 1749–1772. https://doi.org/10.1016/j.rse.2007.08.018.

[36] Dong Y., Milne A.K., Forster B.C.: *A review of SAR speckle filters: texture restoration and preservation*. [in:] *IGARSS 2000. IEEE 2000 International Geoscience and Remote Sensing Symposium. Taking the Pulse of the Planet: The Role of Remote Sensing in Managing the Environment. Proceedings (Cat. No.00CH37120)*, vol. 2, IEEE, 2000, pp. 633–635. https://doi.org/10.1109/IGARSS.2000.861654.

[37] Touzi R.: *A review of speckle filtering in the context of estimation theory*. IEEE Transactions on Geoscience and Remote Sensing, vol. 40(11), 2002, pp. 2392–2404. https://doi.org/10.1109/TGRS.2002.803727.

[38] Lee J.S., Jurkevich L., Dewaele P., Wambacq P., Oosterlinck A.: *Speckle filtering of synthetic aperture radar images: A review*. Remote Sensing Reviews, vol. 8(4), 1994, pp. 313–340. https://doi.org/10.1080/02757259409532206.

[39] Fan X., Liu Y., Wu G., Zhao X.: *Compositing the Minimum NDVI for Daily Water Surface Mapping*. Remote Sensing, vol. 12(4), 2020, 700. https://doi.org/10.3390/rs12040700.

[40] Chen Q., Zhang Y., Ekroos A., Hallikainen M.: *The role of remote sensing technology in the EU water framework directive (WFD)*. Environmental Science & Policy, vol. 7, 2004, pp. 267–276. https://doi.org/10.1016/j.envsci.2004.05.002.

[41] Nicia P., Bejger R., Sterzyńska M., Zadrożny P., Parzych P., Bieda A., Kwartnik-Pruc A.: *Recovery in soil cover and vegetation structure after ancient landslide in mountain fens under Caltho-Alnetum community and response of soil microarthropods (Hexapoda: Collembola) to natural restoration process*. Journal of Soils and Sediments, vol. 20, 2020, pp. 714–722. https://doi.org/10.1007/s11368-019-02434-z.

[42] Manjusree P., Prasanna Kumar L., Bhatt C.M., Rao G.S., Bhanumurthy V.: *Optimization of threshold ranges for rapid flood inundation mapping by evaluating backscatter profiles of high incidence angle SAR images*. International Journal of Disaster Risk Science, vol. 3, 2012, pp. 113–122. https://doi.org/10.1007/s13753-012-0011-5.

[43] Ovakoglou G., Cherif I., Alexandridis T.K., Pantazi X.-E., Tamouridou A.-A., Moshou D., Tseni X., Raptis I., Kalaitzopoulou S., Mourelatos S.: *Automatic detection of surface-water bodies from Sentinel-1 images for effective mosquito larvae control*. Journal of Applied Remote Sensing, vol. 15(1), 2021, 014507. https://doi.org/10.1117/1.JRS.15.014507.

[44] Dabrowska-Zielinska K., Musial J., Malinska A., Budzynska M., Gurdak R., Kiryla W., Bartold M., Grzybowski P.: *Soil Moisture in the Biebrza Wetlands Retrieved from Sentinel-1 Imagery*. Remote Sensing, vol. 10(12), 2018, 1979. https://doi.org/10.3390/rs10121979.

[45] Kasischke E.S., Melack J.M., Dobson M.C.: *The use of imaging radars for ecological applications – A review*. Remote Sensing of Environment, vol. 59(2), 1997, pp. 141–156. https://doi.org/10.1016/S0034-4257(96)00148-4.

[46] Bourgeau-Chavez L.L., Kasischke E.S., Brunzell S.M., Mudd J.P., Smith K.B., Frick A.L.: *Analysis of space-borne SAR data for wetland mapping in Virginia riparian ecosystems*. International Journal of Remote Sensing, vol. 22(18), 2001, pp. 3665–3687. https://doi.org/10.1080/01431160010029174.